Proceedings of the
4th JSME-KSME Thermal Engineering Conference
October 1-6, 2000, Kobe, Japan

F310

RAREFIED GAS FLOWS IN ROTATING HELICAL CHANNELS

Young-Kyu Hwang*, Joong-Sik Heo and Myoung-Keun Kwon*****

School of Mechanical Engineering, Sungkyunkwan University
300 Chunchun-dong, Jangan-gu, Suwon 440-746, Korea
* Professor, ** Postdoctoral Researcher, *** Graduate Research Assistant

ABSTRACT Numerical and experimental investigations are performed for the rarefied gas flows in pumping channels of a helical-type drag pump. Modern turbomolecular pumps include a drag stage in the discharge side, operating roughly in the pressure range of 10^{-2}~10Torr. The flow occurring in the pumping channel develops from the molecular transition to slip flow traveling downstream. Two different numerical methods are used in this analysis: the first one is continuum approach using the Navier-Stokes equations with slip boundary condition, and the second one is stochastic particle approach through the use of the direct simulation Monte Carlo (DSMC) method. The flows in pumping channels are three-dimensional (3D) in the rotating helical channels. The main difficulty in modeling a 3D case comes from the rotating frame of reference. Thus, trajectories of particles are no longer straight lines. In the present DSMC method, trajectories of particles are calculated by integrating a system of differential equations including the Coriolis and centrifugal forces. Our study is the first instance to analyze the rarefied gas flows in rotating frame in the presence of noninertial effects.

Keywords: Helical-type Drag Pump, Direct Simulation Monte Carlo Method, Molecular Transition Flow

1. INTRODUCTION

A turbomolecular pump (TMP) operates efficiently at very low gas density. Under this condition, it has high compression ratio and pumping speed. Today, molecular drag stages are widely used in conjunction with a TMP in order to improve the pumping performance of it[1]. For example, compound or hybrid molecular pumps have gained wide attention because of their increased pumping throughput and discharge pressure.

The drag pump may be of the Holweck (helical-type) or Siegbahn (disk-type) design. In the present study, the pumping performance of a helical-type drag pump (HTDP) is numerically analyzed. The flow within a pumping channel of a HTDP varies from the slip to the molecular transition regime. Two different numerical methods are used in this flow analysis: one is continuum approach using the Navier-Stokes (N-S) equations with slip boun-dary condition, and the other is stochastic particle approach through the use of the direct simulation Monte Carlo (DSMC) method.

Many investigations have been done toward developing theories of the molecular transition and slip flows in channels of a HTDP. By using the DSMC method, Nanbu *et al.*[2] numerically studied the performance in the molecular transition and slip flow regimes. They found that most of pressure rise occurs near the outlet of the channel.

Sawada[3,4] and Sawada and Nakamura[5] extensively analyzed the pumping mechanism by solving the N-S equations with slip boundary condition. These theoretical and experimental investigations give useful data for the channel design by clarifying the relationships between channel geometries and pumping performance.

Sawada[4] also found that the compression performance is improved by the generation of vortices in the molecular transition regime due to the onset of turbulence in the channel.

Panos *et al.*[6] defined the separation pressure between the viscous and the free molecular state, and they extended Gaede's equation, which was used for the helical single-groove drag pump in the free molecular flow, to the helical multi-groove drag pump in both the viscous and free molecular states.

However, the previous studies[2-6] were limited to the quasi-three-dimensional (Q3D) model. Namely, the three-dimensional (3D) rotating helical channel was considered as a rectangular groove facing a wall, which is linearly moving along the groove; see Fig. 1. In the present study, the rotating helical channels are three-dimensionally modeled to investigate the effect of the Coriolis and centrifugal forces on the pumping performance.

As a validation for our computer code, the present numerical results for Q3D and 3D models are first compared with the previously known numerical and experimental ones obtained by Nanbu *et al*[2]. Of the two models, the 3D model gives more accurate results than does the Q3D model. Our experimental results are also presented in the pressure range of 0.02~4 Torr and are compared with numerical ones for both models.

The purpose of the present study is to understand the characteristics of the molecular transition flow field existing within rotating channels of a HTDP. For simplification, we do not take into account complicated physical processes such as rotational and vibrational nonequilibrium. The present numerical results provide information on the velocity and density fields. Finally, we assess the validity and usefulness of the N-S simulations in the molecular transition regime. Particular attention is, therefore, given to the computational limitations of this method.

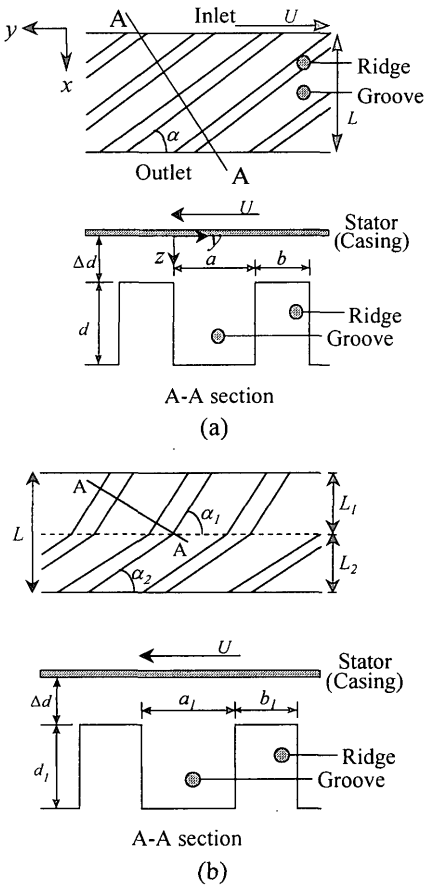

Fig. 1 Geometry of helical-type drag pump (Q3D): (a) rotor 1; (b) rotor 2.

2. Q3D AND 3D MODELS

Helical channels (Q3D) are cut in the axial direction and expanded in the circumferential direction, as seen in Fig. 1. It is convenient to treat the problem within the frame of reference of moving blades. If the coordinate system is fixed with the rotor, the casing is linearly moved from right to left with the velocity U. Two different kinds of rotors are illustrated in Figs. 1(a) and 1(b), respectively. In these figures, α is the helix angle, a the channel width, b the ridge width, d the channel depth, and Δd the clearance between rotor and stator. The channel depth of rotor 1 is 4 mm, while that of rotor 2 is continuously varied from 8 mm (at inlet) to 4 mm (at outlet). Also, the channel shape of rotor 2 consists of two parts, *i.e.*, $\alpha_1 = 40°$ for the upper part of channel and $\alpha_2 = 15°$ for the lower one, respectively.

The former investigations[2-6] did not take into account that there are different effects on the pumping characteristics when the helical channels are set on the rotor or on the stator. Although the performance is quite different for these two cases, the previous Q3D model was considered as equivalent for both cases. In this paper, we present the 3D model to show the effect of the Coriolis and centrifugal forces on the pumping performance. Figures 2(a) and 2(b) illustrate the computational grid of the 3D channel for rotors 1 and 2, respectively.

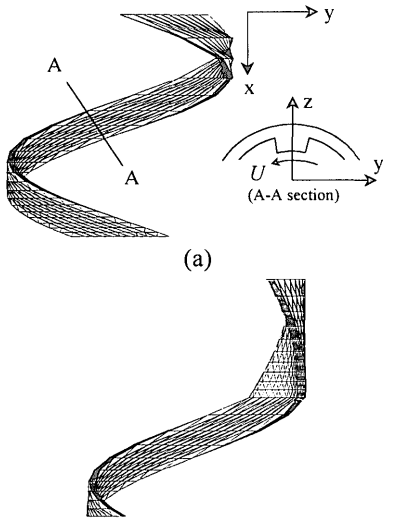

Fig. 2 Computational grid system of 3D helical channel: (a) rotor 1; (b) rotor 2.

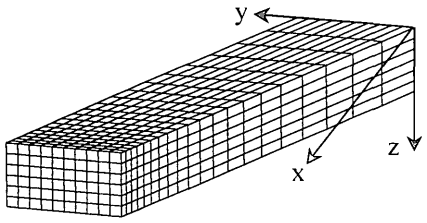

Fig. 3 Computational cells for Q3D model.

3. COMPUTATIONAL METHODS AND BOUNDARY CONDITIONS

The flow conditions considered in the present investigation range from the molecular transition to the slip flow regime. Two different methods are used. The first one is the continuum approach, in which the N-S equations with slip boundary conditions are solved numerically. These equations can be extracted from the Boltzmann equation by retaining terms up to the first order using the Chapman-Enskog expansion[7]. Because the expansion parameter is, essentially, a local Knudsen number Kn, the N-S method becomes inappropriate for large Kn. Thus, we are to clarify the boundary, for this approach, with respect to the rarefaction effects. The second method is the molecular approach, in which a direct physical simulation is performed by considering interactive motions of molecules. The DSMC method of Bird[7] is employed to solve the problem of internal rarefied flows in pumping channels.

To save space, we do not discuss here the procedures in obtaining solutions of the N-S equations; but we refer the reader to Sawada[3,4] and Sawada and Nakamura[5].

The simulated physical space is divided into a network of cells. A rectangular grid system is used in Q3D model, as seen in Fig. 3. In the case of 3D model, the computational grid consists of deformed hexahedral cells, *i.e.*, the four corners of a cell face may not be coplanar. Therefore, each cell is subdivided into five tetrahedral subcells, which have four well-defined triangular faces, to enable tracking the molecules from one cell to another; see Fig. 2. In most of our calculations, the number of cells are

$40\times20\times10$ in the $x-$, $y-$, and $z-$directions, respectively. More grid points are placed near the outlet region of the channel to handle large pressure gradient.

A representative set of particle histories is generated to obtain a good approximation to the molecular distribution function. The essential DSMC approximation is the uncoupling, over a small time interval, of the molecular motions and the intermolecular collisions. Time is advanced in discrete steps of magnitude Δt, which is small compared to the mean collision time between molecules. A large number of molecules is uniformly distributed in the computational domain, and the initial velocities of molecules are evaluated from the Maxwellian distribution function. The gas flows entering the open boundary of the computational domain are initially assumed to be in equilibrium, with zero bulk velocity. The bulk velocity is updated by iteration.

The null-collision technique of Koura[8] is adopted to determine the number of collision pairs selected within a cell during Δt. The collision process is accounted by using the variable soft sphere molecular model of Koura and Matsumoto[9]. The flow field is sampled every 5 time steps during 20000 time steps after reaching the steady state. At the steady state of the simulation, the total number of simulated molecules in the flow domain is about 2×10^5.

The main difficulty in modeling a 3D case comes from the rotating frame of reference. In particular, trajectories of particles are not straight lines in the rotating frame. Thus, trajectories are calculated by integrating a system of differential equations, including the Coriolis and centrifugal forces. The fourth-order Runge-Kutta algorithm is used to integrate the following equation:

$$a_r = -\omega\times(\omega\times r_{mol}) - 2\omega\times V_{mol}, \qquad (1)$$

in which a_r is the relative acceleration, r_{mol} and V_{mol} is the trajectory and the relative velocity of molecules, and ω is the angular velocity of the rotor. From Eq. (1) we can find the position and the velocity of particles at any time on the $y-z$ plane; see Fig. 2.

4. EXPERIMENTAL APPARATUS

Experiments on the pumping characteristics are carried out by using the test pump to verify the present numerical results. The rotor is 168.6 mm in diameter and 132 mm in axial length. It has seven threaded rectangular grooves. The schematic diagram of the experimental apparatus is shown in Fig. 4. This apparatus mainly consists of two parts: the test pump, and instruments that facilitate pressure measurements and flow supply into the test pump. The test pump is connected to a two-stage oil rotary pump (970 *l/min*). The pressure in the high-vacuum side is measured with a Pirani (7.6×10^{-4}~7.6 Torr) and Penning (7.6×10^{-8}~7.6×10^{-3} Torr) gauges, and the pressure in the fore-vacuum side is measured with a Pirani gauge. Experiments are performed by varying the outlet pressure P_2 in the range of 0.02 Torr $\le P_2 \le$ 4 Torr. Test gas (N_2) is supplied through a mass flow controller from a regulated high-pressure cylinder. The motor casing is cooled by water at 22±3℃ during operation.

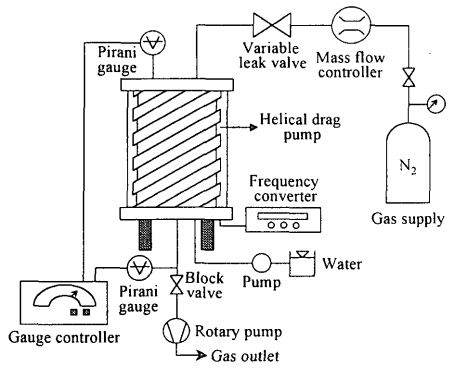

Fig. 4 Schematic diagram of experimental apparatus.

5. RESULTS AND DISCUSSION

To validate our computer program, the present numerical results are compared with the previously known numerical and experimental ones obtained by Nanbu *et al*[2]. The performance curves are shown in Fig. 5. The computations are conducted by employing the DSMC and N-S methods by changing the inlet pressure P_1 for the fixed outlet pressure P_2=0.3 Torr. The present DSMC results for Q3D model agree well with those of Nanbu *et al.* But the N-S results deviate from those of the DSMC method. The throughput Q increases linearly as the pressure difference ΔP ($=P_2-P_1$) decreases. The DSMC results for Q3D model underestimate by as much as 20% in the throughput at ΔP=0.1 Torr comparing with the experimental data. This discrepancy is partly related to a motion between the rotor and casing wall, which is assumed to be linear in Q3D model.

Also, the DSMC results for 3D model are shown in Fig. 5. In the case of Q3D model, only the moving effect of the casing wall on the performance exists; however, in the 3D model, Coriolis and centrifugal forces are dominant effects along with the curvature of channels. In the present study, these effects on the pumping performance are considered. In particular, trajectories of particles are calculated by integrating the system of differential equations, including the Coriolis and centrifugal forces. Consequently, it is seen that the DSMC results which employ 3D model give the best correspondence to the experimental data.

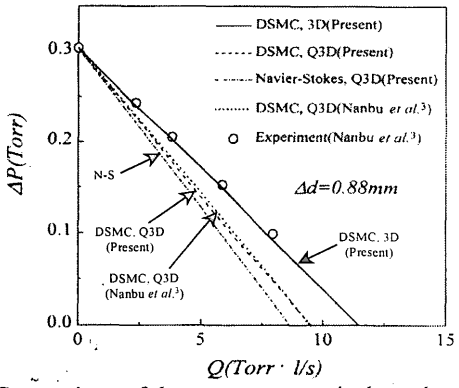

Fig. 5 Comparison of the present numerical results with the previously known ones at P_2=0.3 Torr.

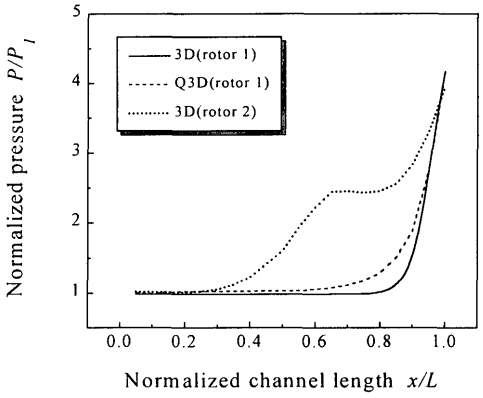

Fig. 6 Pressure distribution obtained by the DSMC method along the pumping channel at P_1=0.023 Torr and P_2=0.1 Torr.

The variations of pressure along the helical channel at P_1=0.023 Torr and P_2=0.1 Torr are shown in Fig. 6, in which the pressure and the length are normalized by the inlet pressure P_1 and the axial length of the helical rotor L, respectively. In the case of rotor 1, the pressure is continuously increased with flow through the channel, and most of the pressure rise occurs near the outlet.

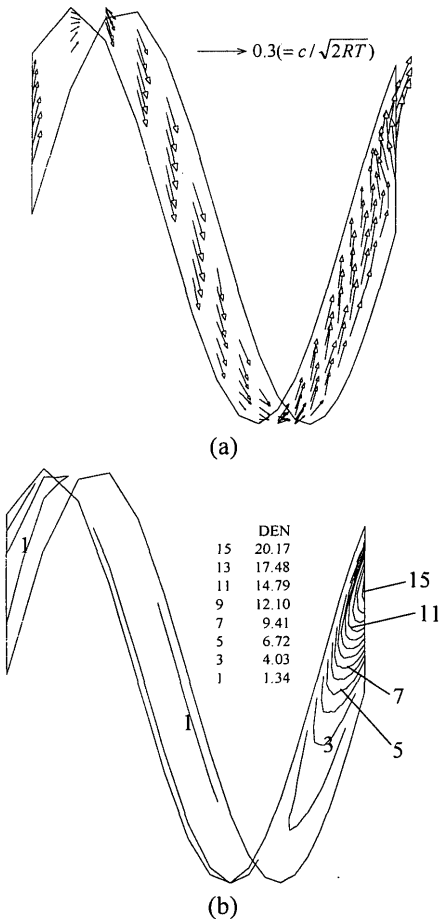

Fig. 7 Flow field obtained by the DSMC method of 3D helical channel (rotor 1) at P_1=0.023 Torr and P_2=0.1 Torr: (a) velocity vectors; (b) density contours.

Especially, it can be seen that the use of 3D model leads to a sharper rise in pressure near the outlet compared to the Q3D model. In the case of rotor 2, the pressure profile becomes flat in the middle of the lower part of channel.

To investigate the detailed flow structure, the relative velocity and density fields for rotor 1 are illustrated in Fig. 7. The pressure conditions are P_1=0.023 Torr and P_2=0.1 Torr. Velocity vectors show a backstreaming of molecules near the channel outlet. Density contours show that the gas density increases rapidly very near the channel outlet. Figure 8 shows velocity vectors and density contours for rotor 2. The pressure conditions are the same as in Fig. 7.

The flow field on the $y-z$ plane is presented in Figs. 9 and 10. We present 4 velocity and density profiles in each figure, respectively, to see the evolution along the channel length. In these figures, the numbers ①, ②, ③, and ④ represent the $y-z$ plane corresponding to the axial location at $x=L/4$, $L/2$, $3L/4$, and L, respectively. We can see the effect of decreasing local Kn on velocity and density profiles. The density contours, as seen in Figs. 9(b) and 10(b), show that the density gradients in the pressure side (P-S) of flow channel are larger than those in the suction side (S-S).

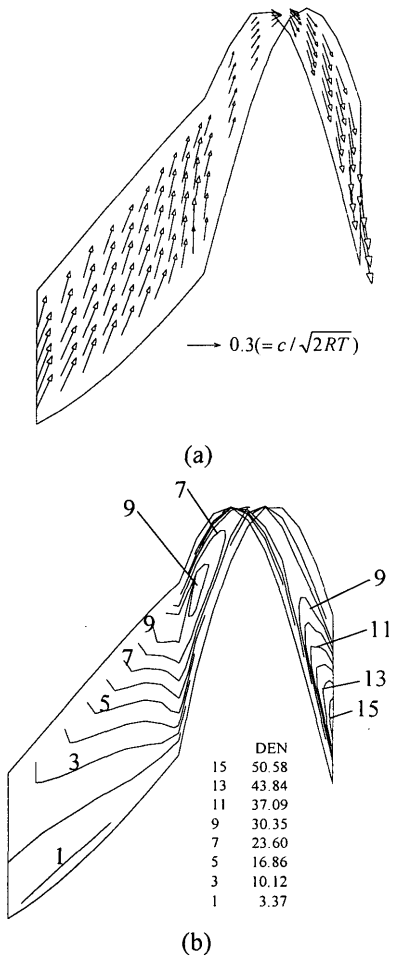

Fig. 8 Flow field obtained by the DSMC method of 3D helical channel (rotor 2) at P_1=0.023 Torr and P_2=0.1 Torr: (a) velocity vectors; (b) density contours.

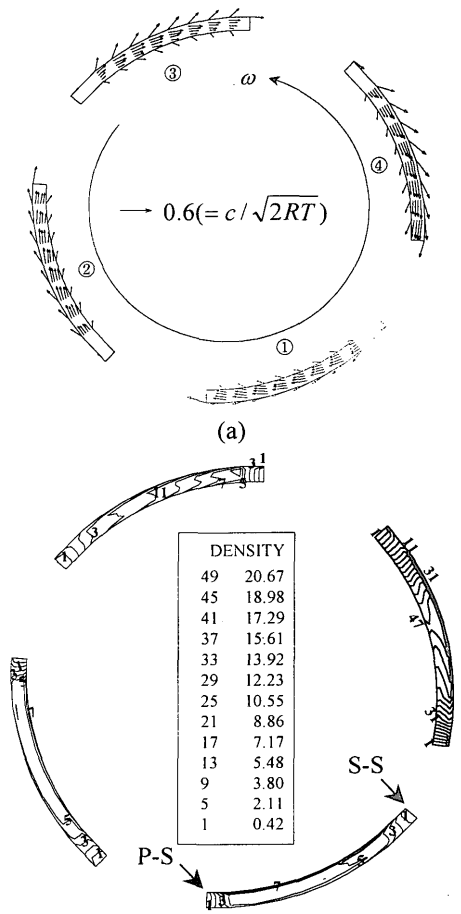

Fig. 9 Flow field obtained by the DSMC method of 3D helical channel at P_1=0.023 Torr and P_2=0.1 Torr: (a) velocity vectors; (b) density contours.

Figure 11 shows the evolution of the conductance, C/C_{fm}, versus the inverse Kn, based on the channel depth and the average pressure $P_a = (P_1 + P_2)/2$. Here, C_{fm} is the free molecular conductance. We obtain a pronounced Knudsen minimum of the conductance around the Kn of 1.

The effect of the outlet pressure on the inlet pressure at zero-flow condition is shown in Fig. 12 for rotor 1. Comparison between the experimental data and the N-S results shows good agreement in the range of $P_2 \geq 2$ Torr. But the discrepancy between the two results becomes larger for $P_2 \leq 1.14$ Torr, *i.e.*, $Kn \geq 0.01$. This indicates that the slip flow analysis of the N-S method is inappropriate for $Kn \geq 0.01$.

Sawada[3,4] showed that the N-S equations can be solved numerically for a rectangular groove with moving wall in the slip flow regime if the boundary conditions are modified to include a slip velocity at the wall. From the momentum transfer between gas and wall, the slip on the wall surfaces is given by:

$$u_s = u_w + Kn\left(\frac{\partial u}{\partial n}\right)_w + \frac{Kn^2}{2}\left(\frac{\partial^2 u}{\partial n^2}\right)_w, \qquad (2)$$

where u_s and u_w refer to the slip velocity and the wall velocity, respectively.

As seen in Fig. 12, the results obtained by the second-order modification are the same as those obtained by the first-order slip velocity in the range of $P_2 > 1$ Torr. The differences between the two results appear noticeably for $P_2 < 0.1$ Torr. Although the second-order modification fails to predict quantitatively the experimental data as in the first-order method, it is interesting to note that the results obtained by the second-order method agree qualitatively with the experimental data.

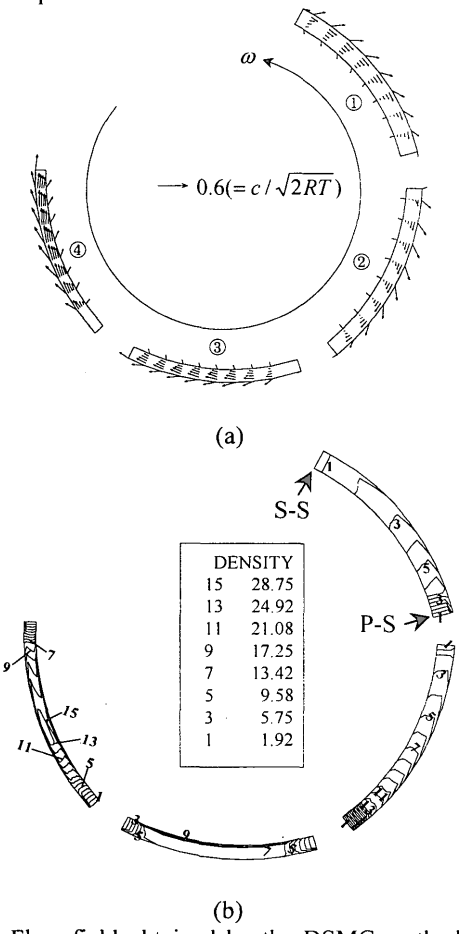

Fig. 10 Flow field obtained by the DSMC method of 3D helical channel at P_1=0.023 Torr and P_2=0.1 Torr: (a) velocity vectors; (b) density contours.

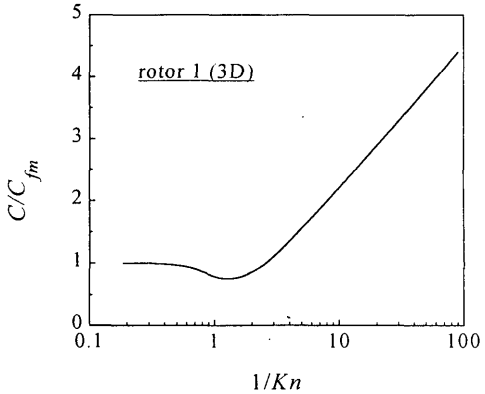

Fig. 11 Inverse Knudsen number effects on the conductance through the channel from molecular to slip flow regime.

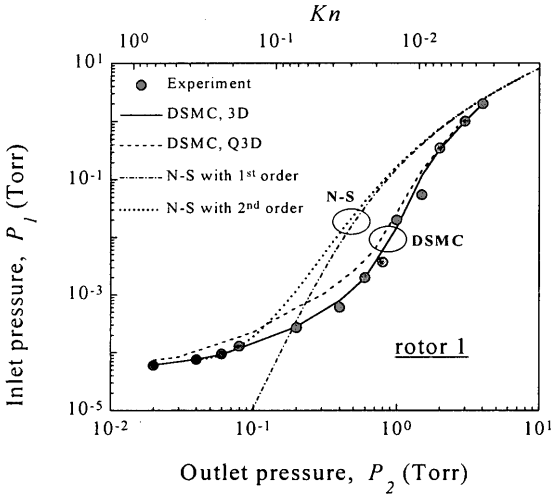

Fig. 12 Effect of the outlet pressure on the inlet pressure at zero throughput.

Experimental results are compared with those obtained by the DSMC simulations. The good agreement between the two is shown in Fig. 12. This clearly reveals the ability of the DSMC method to predict the molecular transition flows. Especially, the 3D model predicts well the experimental data.

6. CONCLUSIONS

Numerical and experimental studies have been made for the molecular transition and slip flows in the rotating helical channel of a HTDP. The computations are conducted by employing the N-S and DSMC methods. The present results obtained by both methods agree well with the experimental data for $Kn \le 0.01$. In particular, the N-S method with slip boundary conditions drastically simplifies the simulation and saves computational effort in predicting the performance for this regime. But, the results from the DSMC method are only reasonable in the molecular transition regime for $Kn \ge 0.01$. A new 3D model of a helical channel has been developed, and the effects of the Coriolis and centrifugal forces on the pumping performance are discussed. The results indicate that the present 3D model gives more accurate solutions than does the previous Q3D model.

7. REFERENCES

1. Hablanian, M. H., Vacuum Science and Technology: Pioneers of 20th Century, (1994), AIP, New York.
2. Nanbu, K., Kubota, H., Igarashi, S., Urano, C. and Enosawa, H., Performance of Spiral Grooves on a Rotor of Turbomolecular Pump, Trans. JSME, Vol. 57, No. 533, (1991), pp. 172-177.
3. Sawada, T., Vacuum Sealing with a Spiral Grooved Gas Dynamic Seal, Bull. JSME, Vol. 22, No. 169, (1979), pp. 974-981.
4. Sawada, T., Improvement in the Performance of Spiral Grooved Visco-Vacuum Pumps in the Coarse Vacuum Region, Vacuum, Vol. 44, No. 5-7, (1993), pp. 689-692.
5. Sawada, T. and Nakamura, M., Spiral Grooved Visco-Vacuum Pumps with Various Groove Shapes, Vacuum, Vol. 41, No. 7-9, (1990), pp. 1833-1836.
6. Panos, C. N., Antoniou, A. G. and Valamontes, S. E., The Helicoid Multi-Groove Vacuum Pump in Both Viscous and Molecular States, Vacuum, Vol. 45, No. 8, (1994), pp. 841-847.
7. Bird, G. A., Molecular Gas Dynamics and the Direct Simulation of Gas Flows, (1994), Clarendon Press.
8. Koura, K., Null-collision Technique in the Direct Simulation Monte Carlo Method, Phys. Fluids, Vol. 29, No. 11, (1986), pp. 3509-3511.
9. Koura, K. and Matsumoto, H., Variable Soft Sphere Molecular Model for Air Species, Phys. Fluids, Vol. 4, No. 5, (1992), pp. 1083-1085.

Acknowledgement

This work was supported by the Brain Korea 21 Project.

NOMENCLATURE

a	channel width (mm)
a_r	relative acceleration (m/s^2)
b	ridge width (mm)
C	conductance (m^3/s)
d	channel depth (mm)
Δd	clearance (mm)
Kn	Knudsen number, λ / d
L	axial length of rotor (mm)
P	pressure (Pa)
P_a	average pressure, $(P_1 + P_2)/2$
Q	throughput (Pa ° *l*/s)
r_{mol}	trajectory of molecules
R	ordinary gas constant
T	absolute temperature (K)
u	velocity (m/s)
U	peripheral speed of rotor (m/s)
V_{mol}	relative velocity of molecules (m/s)

Greek symbols

α	helix angle of channel
λ	mean free path (mm)
μ	dynamic viscosity (Pa ° s)
ω	angular velocity (rad/s)

Subscripts

1	inlet
2	outlet
fm	free molecular
s	slip
w	wall